

Aerodynamic Cross-coupling in a Flexible Rotor: Control Design and Implementation

Simon E. Mushi¹ Zongli Lin¹ Paul E. Allaire² and Stephen Evans²

¹Charles L. Brown Department of Electrical and Computer Engineering

²Department of Mechanical and Aerospace Engineering

University of Virginia, Charlottesville, VA 22904, U.S.A.

Email: {sem5t,zl5y,pea,sme9s}@virginia.edu

Abstract—This paper is concerned with modeling and active vibration control of a 1.23-m long flexible shaft on active magnetic bearings that is designed to model a small industrial compressor and to serve as a platform for investigating emerging control schemes. Aerodynamic cross-coupled stiffness is one of the main contributors to rotordynamic instability in modern turbo-machines. The destabilizing effects of the cross-coupled stiffness are demonstrated. H_2 and H_∞ synthesis approaches are used to design controllers that may stabilize the rotor-bearing system over a wide range of cross-coupled stiffness. Stability analysis and dynamic simulations of the resulting closed-loop systems are performed and recommendations made on the best means of achieving the desired performance and stability of the rotor-bearing system. The control and data-acquisition are in the process of being implemented in real-time using a DSP system.

Index Terms—Keywords: Active magnetic bearings, Cross-coupled stiffness, Robust control, Real-time systems

I. INTRODUCTION

Active magnetic bearings (AMBs) represent an exciting alternative to existing mechanical bearing designs in a variety of turbo-machines. Low power loss, contact-free dynamics, high-speed operation, direct control of forces on the rotor leading to lower vibration levels, lower maintenance costs and longer system life are all well understood advantages of implementing an AMB system [1]. Much of the effort to realize these gains lies in the design of the control law and accompanying sensor and actuator electronics.

Aerodynamic cross-coupling forces in industrial compressors and turbines are a result of fluid structure interactions produced by flow differences in clearances around centrifugal impellers and gas/liquid seals, hydrodynamic bearings [2], [3]. The sub-synchronous, non-conservative and self-exciting nature of these forces is of major concern to machinery designers and operators as they create potentially unstable rotor vibrations, which can lead to serious machine damage when insufficient damping is available [2], [5]. While some theoretical models for the factors that contribute to cross-coupling are available, generally they are not very accurate. A further complexity arises when parametric and non-parametric dynamics are introduced, e.g., speed-dependent gyroscopic behavior. This parameter varying control problem provides an opportunity for the dynamic properties of AMB suspension to assure robust stability in many cases. Adaptive control schemes using the have been applied to the problem of cross-

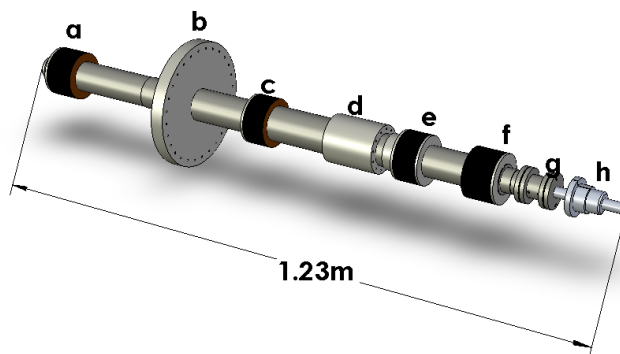


Figure 1. A 3-D model of the test-rig shaft showing support AMB lamination stacks (a,f), disturbance AMB lamination stacks (c,e), gyroscopic disks (b,d), a flexible disc pack coupling (g) and drive attachment (h).

coupled stiffness in rotor-AMB systems, however they have been limited to small rigid rotors [6], [7], [8].

Our goal is to design and build a test bed with a flexible, gyroscopic rotor mounted on AMBs, subject to destabilizing cross-coupling stiffness and design a high performance controller to provide robust stability. In producing a test rig of a scale similar to a small industrial compressor, we are to examine some of the challenges seen in industry and investigating the development of appropriate industrial specifications into valid control design objectives.

The test rig we are constructing has a 1.23m long steel shaft weighing 440N with a maximum running speed of 14,200RPM. As shown in Fig. 1, four laminated Si-Fe bushings are mounted with a locational interference shrink fit onto the shaft for attraction by the non-drive end (a) and drive-end (f) radial support AMBs and the two radial (c,e) disturbance AMBs. The bearings operate with a 0.38mm air gap and each has a peak load capacity of 800N [9]. This combination of AMBs allows either between-bearing or overhung rotor configurations, potentially representing axial and centrifugal compressor designs, to be realized. In addition, two discs (b,d) of different diameters are mounted on the shaft to mimic a typical compressor rotor blade arrangement. Disc b would serve as a dual purpose of a thrust AMB collar for controlling axial motion. Eddy current displacement sensors (Kaman Measuring Systems) are differentially mounted in close proximity to each bearing bushing to reduce non-collocation and spillover

problems. A flexible disk pack coupling is used to mitigate the effect of angular and offset misalignment between the drive shaft and the test rig. Copley Controls models 413 and 422 analog switching power amplifiers were selected to drive the bearing coils based on the power output required to generate the calculated maximum available force slew rate. Real-time digital control is implemented using a PC-based DSP solution, the M6713 board (Innovative Integration, Simi Valley, CA).

II. SYSTEM MODELING

A. Rotordynamics

A high fidelity finite element rotor model containing 49 nodes was constructed for the plant model to determine critical speeds and mode shapes using a custom FEM package. The first bending mode for the free-free shaft was calculated at 11,400 RPM. The resulting critical speed map and free-free rotor mode shapes are shown in Figs. 2 and 3, respectively. Each node was assigned 4 physical degrees of freedom, representing translations in the x - and y -directions and angular displacements about the xz (θ_y) and yz (θ_x) planes. This generates entries for the mass (M), internal shaft stiffness (K_s), damping (C) and gyroscopic (G) global matrices to enable the Lagrangian representation of the second order dynamical system,

$$M\ddot{q} + (C + \omega G)\dot{q} + K_s q = F_m + F_u + F_w \quad (1)$$

where

$$q = [x_1 \ \theta_{y_1} \ \dots \ x_n \ \theta_{y_n} \ y_1 \ \theta_{x_1} \ \dots \ y_n \ \theta_{x_n}]^T$$

is the 196×1 system state vector, F_m represents the force due to the AMBs, F_u represents the synchronous excitation force due to rotor imbalance, and F_w represents external disturbances, e.g., destabilizing cross-coupling stiffness, static and dynamic loads. Reduction of the plant order is necessary to facilitate a practical control design. A planar modal coordinate transformation was chosen to preserve the first 7 modes representing an approximately 3.5kHz bandwidth that is within the power bandwidth of the PWM amplifiers. This transformation ($\tilde{q} = Tq$) is determined by solving the free-free undamped eigenvalue problem for a real matrix T , the subset of eigenvectors corresponding to the modes to be retained. Eqn (1) is then replaced by the following,

$$T^T M T \ddot{\tilde{q}} + T^T (C + \omega G) T \dot{\tilde{q}} + T^T K_s T \tilde{q} = T^T (F_m + F_u + F_w) \quad (2)$$

and the resulting model now has 10 states.

B. Linearized cross-coupling stiffness model

Using a linear model for the aerodynamic cross-coupled stiffness generated by the AMB at the shaft mid-span, the effective cross-coupling force is calculated by,

$$F_{xc} = -\chi \begin{bmatrix} 0 & 1 \\ -1 & 0 \end{bmatrix} \begin{bmatrix} q_{x_{mid}} \\ q_{y_{mid}} \end{bmatrix} = -\chi K_{xc} q \quad (3)$$

The magnitude of the cross-coupling effect is controlled by a scalar χ varying between 0 and 40MN/m [7].

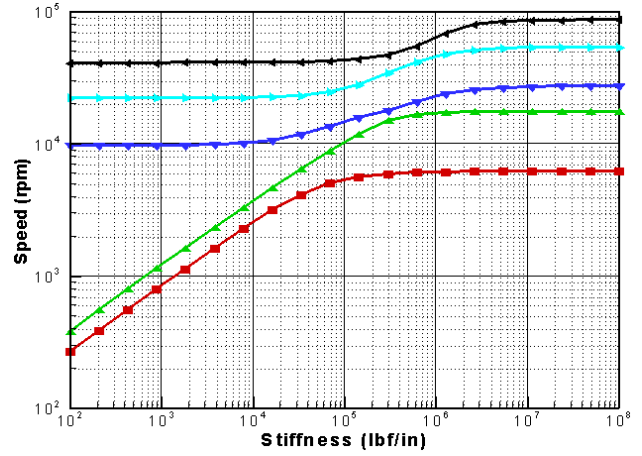


Figure 2. Critical speed map for the rotor.

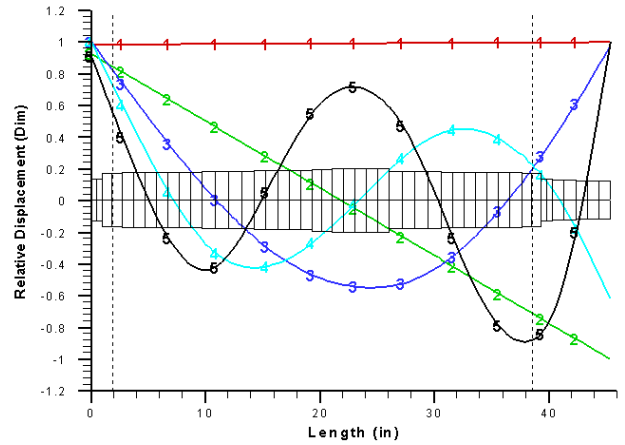


Figure 3. The first five free-free rotor mode shapes.

C. Rotor-bearing model

Using a linear magnetic bearing model [10] with nominal current stiffness ($K_i = 191.8N/A$) and position stiffness ($K_x = 2.62 \times 10^6 N/m$), we can express the force provided by the support AMB as,

$$F_m = K_i i + K_x x \quad (4)$$

The unbalance force, F_u , as a result of residual rotor imbalance at discs b and d (see Fig. 1), is calculated as

$$F_u = m e_u \omega^2 \cos(\omega t) + m e_u \omega^2 \cos(\omega t + \theta) \quad (5)$$

where m is the shaft mass, $e_u = 250\mu\text{m}$ -mm the unbalance eccentricity as per the API 617 specification for centrifugal compressors, ω the shaft rotation speed, and θ the phase lag between the phasors representing the unbalance force vector at each disc. Finally, a state-space formulation of the dynamic system in Eqn (1) is the presented below

$$\dot{x}_r = A_r x_r + B_{r_i} i + B_{r_w} w \quad (6)$$

$$y = C_r x_r \quad (7)$$

where,

$$A_r = \begin{bmatrix} 0 & I \\ -M_r^{-T}\Pi M_r^{-1} & -M_r^{-T}(C_c + \omega G_c)M_r^{-1} \end{bmatrix}$$

$$\Pi = \chi K_{xc} - B_m K_x B_m^T + K_s$$

$$B_{r_i} = \begin{bmatrix} 0 \\ M_r^{-T} B_m K_i \end{bmatrix}$$

$$B_{r_w} = \begin{bmatrix} 0 \\ M_r^{-T} B_w \end{bmatrix}$$

$$C_r = \begin{bmatrix} C_m M_r^{-1} & 0 \end{bmatrix}$$

with B_m and C_m being the coefficient matrices for the control actuator input and displacement measurement output, respectively. To arrive at this first-order form, the symmetric global mass matrix M is eliminated by Choleski factorization ($M = M_r^T M_r$) and the following transformations performed [11],

$$x_r \triangleq M_r q \quad C_c \triangleq M_r^{-T} C M_r^{-1} \quad G_c \triangleq M_r^{-T} G M_r^{-1}.$$

D. Sensor and amplifier models

The eddy current displacement sensors are modeled as a first order system with a gain ($K_s = 8\text{mV}/\mu\text{m}$) and cut-off ($\omega_a = 20\text{kHz}$) corresponding to the sensitivity and bandwidth of the probe heads. For a single differential probe arrangement, the transfer function from displacement to voltage output is,

$$\frac{v_s}{y} = K_s \frac{\omega_a}{s + \omega_a} \quad (8)$$

The transfer functions for all the sensors are then combined into a single state space model with the following labels,

$$G_s(s) : \begin{pmatrix} A_s & B_s \\ C_s & D_s \end{pmatrix} \quad (9)$$

The PWM amplifiers are modeled using transconductance, where a control voltage (u) is suggested by the controller and a desired current (i_c) is supplied to the AMB coils. The amplifiers have an internal feedback loop to ensure the target current is realized. The power bandwidth of the amplifiers is affected by the largely inductive AMB coil impedance. The following is a transfer function for a single amplifier actuating in one degree of freedom

$$\frac{i_c}{u} = \frac{K_{pa}}{L_c + R_c + \gamma K_{pa}} \quad (10)$$

where K_{pa} is the amplifier reference gain, γ is the current feedback sensitivity, and R_c and L_c are the resistance and inductance of a single AMB control quadrant, respectively. All these parameters are obtained experimentally. As with the sensors, the transfer functions for all 8 amplifiers (2 amplifiers / DOF) have a state-space representation as,

$$G_a(s) : \begin{pmatrix} A_a & B_a \\ C_a & D_a \end{pmatrix} \quad (11)$$

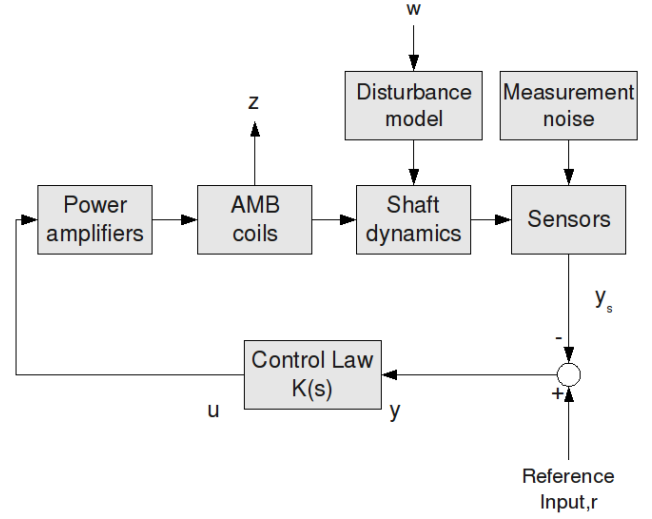


Figure 4. System overview.

E. Generalized plant

The MIMO system model representing the combined rotor-bearing-amplifier-sensor model has 4 control inputs ($u = [v_{x_1} v_{y_1} v_{x_2} v_{y_2}]^T$), 4 measured outputs ($y = [y_{x_1} y_{y_1} y_{x_2} y_{y_2}]^T$), and 28 states comprising 20 modal reduced shaft states (x_r), and the remaining from the amplifier (x_a) and sensor (x_s) models. In addition there are 12 exogenous inputs ($w = [w_1 \dots w_{16}]^T$) used to introduced external forces onto 12 pre-determined shaft locations. For example, several of the disturbance inputs are used to introduce synchronous unbalance excitations, and other inputs to produce static force loads on the shaft. The performance metric ($z = [i_{x_1} i_{y_1} i_{x_2} i_{y_2}]^T$) consists the estimated control currents generated in each AMB. An overview showing the interconnection of the models and the flow of signals is shown in Fig. 4.

The generalized plant, $G(s)$, can then be outlined as,

$$G(s) : \begin{bmatrix} \dot{x}_r \\ \dot{x}_s \\ \dot{x}_a \\ z \\ y \end{bmatrix} = \begin{bmatrix} A_r & 0 & B_{r_i} C_a & B_{r_w} & 0 \\ B_s C_r A_s & 0 & 0 & 0 & 0 \\ 0 & 0 & A_a & 0 & B_a \\ 0 & 0 & C_a & 0 & 0 \\ 0 & C_s & 0 & 0 & 0 \end{bmatrix} \begin{bmatrix} x_r \\ x_s \\ x_a \\ w \\ u \end{bmatrix} \quad (12)$$

With more compact notation we represent the plant with the following state-space representation,

$$G(s) : \begin{pmatrix} \mathbb{A} & \mathbb{B}_1 & \mathbb{B}_2 \\ \mathbb{C}_1 & \mathbb{D}_{11} & \mathbb{D}_{12} \\ \mathbb{C}_2 & \mathbb{D}_{21} & \mathbb{D}_{22} \end{pmatrix} \quad (13)$$

where

$$\mathbb{A} = \begin{bmatrix} A_r & 0 & B_{r_i} C_a \\ B_s C_r A_s & 0 & 0 \\ 0 & 0 & A_a \end{bmatrix}$$

$$\mathbb{B}_1 = \begin{bmatrix} B_{r_w} \\ 0 \\ 0 \end{bmatrix}, \mathbb{B}_2 = \begin{bmatrix} 0 \\ 0 \\ B_a \end{bmatrix}$$

$$\mathbb{C}_1 = [0 \ 0 \ C_a], \mathbb{C}_2 = [0 \ C_s \ 0]$$

$$\mathbb{D} = 0$$

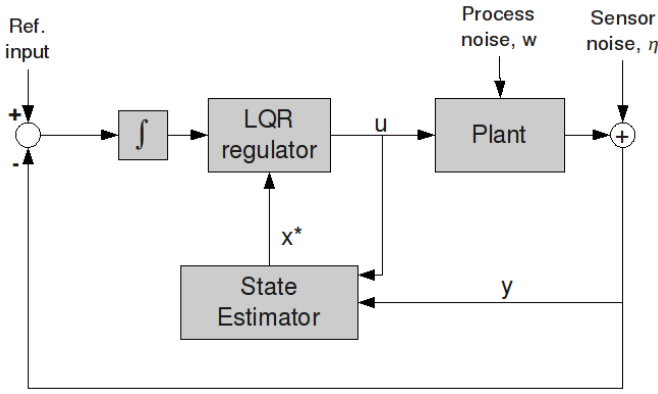


Figure 5. Block diagram of rotor-AMB plant and LQG controller with integral action and reference input.

III. ROBUST CONTROL DESIGN

A. LQG (H_2) synthesis

An optimal control design approach was followed to minimize a quadratic performance index, $J(u)$, and to obtain a linear control law $u = -Kx$. The advantage of this approach is that the performance index can correspond to physical concepts such as time or energy expended by the controller or plant [12]. Linear quadratic (LQ) is a special case of the general H_2 problem and provides a solution for MIMO systems in which tuning of decoupled PID controllers to achieve stability targets is daunting due to the number of parameters for even a simple MIMO system [13]. A general form of the performance index is given by

$$J(u) = \int_0^{\infty} \{x^T Q x + u^T R u\} dt \quad (14)$$

where $Q = Q^T > 0$ and $R = R^T > 0$ are weighting matrices that specify the contribution of state energy and controller input energy to the overall performance index. Minimizing the state energy will reduce the settling time and overshoot of the system, while minimizing the control input energy will reduce the noise sensitivity of the system [12].

We will set R to an identity matrix and vary Q iteratively to find the control law with the best step response, and control gains that are not unacceptably large. Output feedback will be used since a limited number of displacement sensors cannot provide total state information for the rotor-bearing-amplifier system. However, since the system is stabilizable, a Kalman filter can be used to provide state estimates that will converge to the actual plant states, using Gaussian measurement and plant noise models. The combination of linear quadratic regulator (LQR) and Kalman filter is a linear quadratic Gaussian (LQG) control. Fig. 5 provides an overview of the LQG controller with integral action (to eliminate steady state error).

Three controllers, A, B, and C, were synthesized with χ values of 0, 20 and 40MN/m, respectively, covering the range of cross-coupling stiffness expected. These controllers were then used to attempt to stabilize eight different plants with χ over this range. Figs. 6, 7 and 8 show the effect of

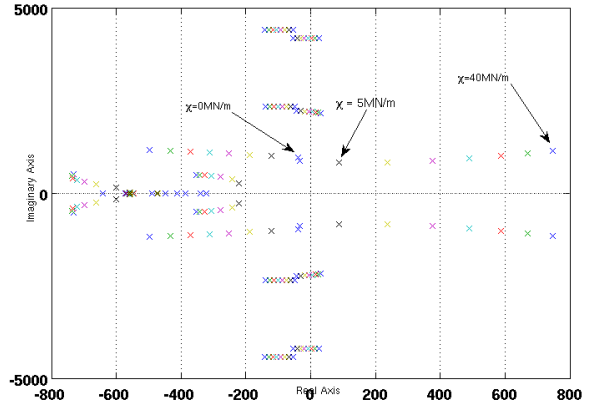


Figure 6. Effect on closed-loop poles of the varying cross-coupling stiffness with LQG controller A (designed at $\chi = 0\text{MN/m}$).

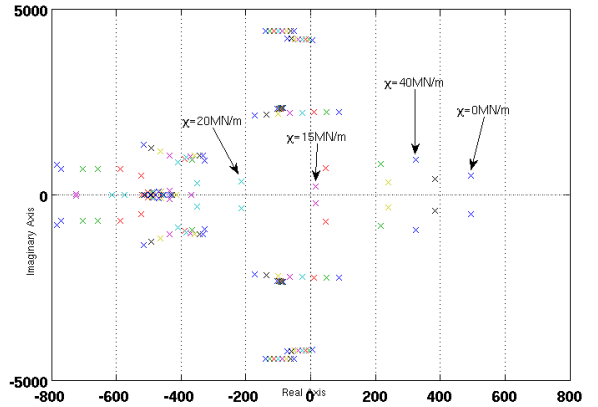


Figure 7. Effect on closed-loop poles of the varying cross-coupling stiffness with LQG controller B (designed at $\chi = 20\text{MN/m}$).

varying cross-coupled stiffness on the closed-loop poles under controllers A, B and C.

B. H_∞ synthesis

The H_∞ norm provides a measure of the worst-case norm (γ) of the transfer function from disturbance input (w) to performance metric (z), $T_{zw}(j\omega)$. In particular, this norm is minimized while ensuring the closed-loop system is stable, thus producing a H_∞ suboptimal controller [13], [14]. The suboptimal H_∞ cost can be represented as,

$$\|T_{zw}\|_\infty \triangleq \sup_{\omega} \sigma_{\max}(T_{zw}(j\omega)) < \gamma \quad (15)$$

As before, three controllers, D, E, and F, were synthesized with χ values of 0, 20 and 40MN/m, respectively, covering the range of cross-coupling stiffness expected. The MATLAB command `hinfsyn` was used to obtain an LTI model of the H_∞ controller. Eight rotor-bearing-sensor-amplifier plants with χ values varying over the specified range were realized and a generalized feedback made with each controller. Figs 9

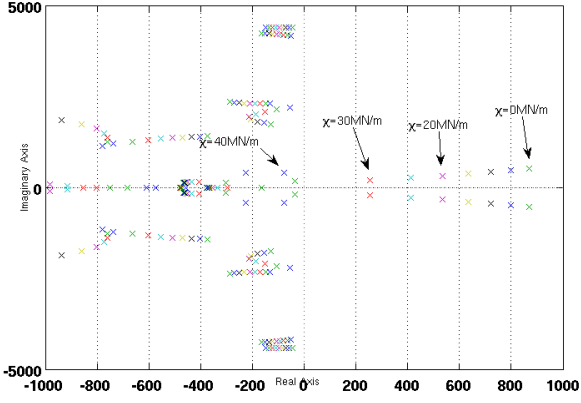


Figure 8. Effect on closed-loop poles of the varying cross-coupling stiffness with LQG controller C (designed at $\chi = 40\text{MN/m}$).

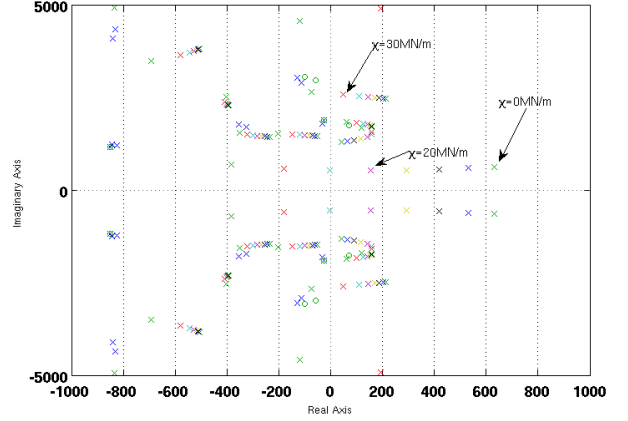


Figure 10. Effect on closed-loop poles of the varying cross-coupling stiffness with H_∞ controller F (designed at $\chi = 40\text{MN/m}$).

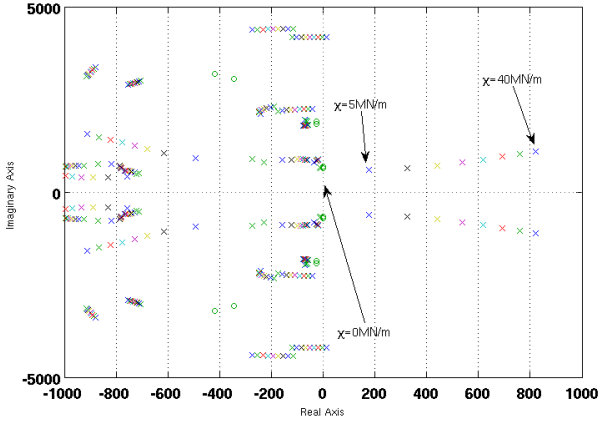


Figure 9. Effect on closed-loop poles of the varying cross-coupling stiffness with H_∞ controller D (designed at $\chi = 0\text{MN/m}$).

and 10 are pole-zero maps of the closed-loop systems using controllers D and F respectively.

IV. DISCUSSIONS

For the LQG controller, it was observed that changing the weighting criteria \mathbb{Q} and \mathbb{R} did not greatly affect the locations of the unstable closed-loop poles. The pole-zero maps for the LQG controller (Figs. 6-8) show that the closed-loop systems only exhibited stability for a limited range of cross-coupled stiffness in the neighborhood of the value of χ that was used in the control design. Using a greater value of χ in control synthesis did not guarantee that all stiffness less the design value would be stabilized. The same was also true of the H_∞ synthesis approach - as Fig. 10 shows that a controller able to stabilize a plant with $\chi = 40\text{MN/m}$ is unable to stabilize the other plants with $\chi = 0 - 30\text{MN/m}$. The plots illustrate the primary drawback of the LQG and H_∞ approaches as executed in this study - lacking a priori knowledge of the nature of the cross-coupling stiffness effect, our control choice is limited. However, there exist additional control strategies

that we anticipate in further work and may enable stabilization over a wider range of cross-coupled stiffness. Two of these are gain scheduling and piece-wise μ -synthesis for robust control.

1) *Gain scheduling*: Gain scheduling of robust controllers with bumpless transfer has been implemented in flywheel AMB systems[15]. In this particular flywheel application a single LTI controller was unable to stabilize the highly gyroscopic rotor over the entire speed range, and hence an innovative means of dynamically switching between multiple robust controllers without a “bump” was demonstrated. A similar approach could be applied to our rotor-AMB system, since we have cross-coupled stiffness as a parameter of a linear parameter varying (LPV) plant and we can “piece” together multiple controllers that would ensure a much larger stability range. An additional challenge to the issues encountered in [15] is the need to determine the value of cross-coupled stiffness at known location(s) on the shaft before the control switching can be performed.

2) *Robust control via μ -synthesis*: The structured singular value, μ , is an important tool in the analysis of uncertain systems as well as in the synthesis of robust controllers [12]. Parametric and/or non-parametric uncertainties present in the plant model are captured through this approach, and can be used to represent the speed-dependent gyroscopics and unknown cross-coupling stiffness present. Techniques such as DK-iteration can be used to synthesize controllers that may satisfy the stability and performance demands of the rotor-AMB system.

V. CONCLUSIONS

This paper presents the modeling of a rotor-AMB system focusing primarily on the effects of unknown cross-coupled stiffness on rotor stability. H_2 and H_∞ control approaches were only able to stabilize the rotor-AMB system when cross-coupled stiffness in a small neighborhood of the designed value. Further work in the direction of gain-scheduled robust control and μ -synthesis is planned to accomplish the goal of expanding the stability range with respect to cross-coupled stiffness.

REFERENCES

- [1] Schweitzer, G., Bleuler, H. and Traxler A., Active Magnetic Bearings: Basics, Properties and Applications of Active Magnetic Bearings, ETH Zurich, 1994.
- [2] Allaire, P.E. and Sheth, MAE 792 Advanced Rotordynamics Course Notes, University of Virginia, Spring 2007.
- [3] Ertas, B. and Vance, J., The influence of same-sign cross-coupled stiffness on rotordynamics, *Journal of Vibration and Acoustics*, Vol 129, pp. 24-31, 2007.
- [4] Inman, D.J., *Vibration with control*, Wiley, Great Britain, 2006.
- [5] Moore, J.J., Ransom, D.L. and Viana, F., Innovative diagnosis for instability in turbo-machinery, *ANSYS Advantage*, Vol 2., Issue 1, pp. 20-22, 2008.
- [6] Wurmsdobler, P., State Space Adaptive Control for a Rigid Rotor Suspended in Active Magnetic Bearings, PhD Dissertation, University of Technology Vienna, Austria, 1997.
- [7] Hirschmanner, M., Steinschaden, N. and Springer, H., Adaptive control of a rotor excited by destabilizing cross-coupling forces, *Proceedings of Sixth International Conference on Rotor Dynamics*, Sydney, Australia, pp. 38-45, 2002.
- [8] Lang, O., Wassermann, J. and Springer, H., Adaptive Vibration Control of a Rigid Rotor supported by Active Magnetic Bearings, *Journal of Engineering for Gas Turbines and Power*, Vol. 118, pp. 825-829, 1996.
- [9] Kasarda, M., The measurement and characterization of power losses in high speed magnetic bearings, PhD. Dissertation, University of Virginia, U.S.A., 1997.
- [10] Allaire, P.E., Maslen, E.H., Humphris, R.R., Knospe, C.R. and Lewis, D.W., "Magnetic Bearings" in *CRC Handbook of Lubrication and Tribology*, vol. III, pp 577-600, 1994.
- [11] Maslen, E.H., Magnetic Bearings, http://www.people.virginia.edu/~ehm7s/MagneticBearings/mag_brgs.pdf. Accessed in January 2007.
- [12] Skogestad, S. and Postlethwaite, I., *Multivariable Feedback Control: Analysis and Design*, 2nd Edition, Wiley, Chichester, U.K., 2005.
- [13] Skelton, R.E., Iwasaki, T. and Grigoriadis, T., *A Unified Algebraic Approach to Linear Control Design*, Taylor and Francis, London, U.K, 1998.
- [14] MATLAB 2008a Control System Toolbox, Robust Control Toolbox. The Mathworks, Inc., Natick, MA, U.S.A.
- [15] Li, G., Allaire, P.E., Lin, Z. and Huang, B., Dynamic Transfer of Robust AMB Controllers, *8th International Symposium on Magnetic Bearings*, Mito, Japan, Aug. 26-28, 2002.